2024 IEEE/RSJ International Conference on Intelligent Robots and Systems (IROS)
October 14-18, 2024. Abu Dhabi, UAE

Tracking Control with Uncertainty Smoothing Estimation under Aggressive Maneuvers of Aerial Vehicles

Hao Zhang[1], Tao Jiang[1], Jianchuan Ye[2], Senqi Tan[3], and Zhi Zheng[1]

***Abstract*— Aggressive maneuvering is crucial for aerial vehicles to execute adversarial and penetration missions. However, this challenges the accurate tracking control of drones due to uncertainties induced by high-speed flight. Therefore, firstly, a highly dynamic tracking control framework is proposed to actualize the accurate tracking of aggressive trajectories with velocities up to 15 m/s (i.e., 54 km/h) and acceleration of 2 g. Secondly, in order to mitigate the impact of conjoint effects on uncertainty estimation during aggressive flights and to ensure that uncertainty is smoothly compensated, a novel adaptive nonlinear extended state observer (ANESO) with noise suppression and peak attenuation capabilities is designed. Finally, extensive comparative simulation and real-world practical experimental results certify the superiority of the proposed control strategy in tracking aggressive trajectories.**

I. INTRODUCTION

RECENTLY, as a representative of drones, the quadrotor has received significant attention [1]–[3]. Utilizing the strong maneuverability and agility of quadrotors to traverse challenging areas at very high speeds and accelerations has become the new competitive frontier. However, the accurate tracking of quadrotors under aggressive maneuvers requires the support of superior control strategies and reliable uncertainty estimation methods.

Tracking control is one of the conditions for autonomous flight of quadrotors [4]–[6]. With assumptions such as small-angle, mature and implementable linear control methods have shown satisfactory capabilities in slow flight or hover control [7]. However, as highly dynamic maneuvering requirements emerge, these assumptions are no longer effective. To achieve accurate tracking of aggressive trajectories, various control methods have been proposed in [8]–[10]. A seminal work [11] revealed that quadrotors are differentially flat systems, and utilizing this feature, differential flatness-based controllers were further developed in [12] and [13]. The predictive properties of nonlinear model predictive controllers are believed to contribute to high-speed trajectory tracking [14]–[16]. However, the computational requirements and possible convergence problems of this method make its practicability in aggressive trajectory tracking worth considering.

Fig. 1. Slow-motion photo. A video demonstration of this article is available at https://youtu.be/5qQR7GbVL0E.

Unlike slow flight, quadrotors are more susceptible to conjoint effects in aggressive flight, i.e., external disturbances, actuator constraints, as well as aerodynamic effects induced by high-speed flight. To mitigate the influence of uncertainty and improve control behavior, various uncertainty estimation schemes have been developed in [17], [18]. As an effective representative of uncertainty estimation, extended state observer (ESO) [19] is widely used in practice. Unfortunately, for ESO, the high gain makes it sensitive to measurement noise. For that, estimation structures [20], [21] that combine filters with ESOs have emerged. However, these combination strategies are subject to filter performance constraints. In addition, to improve the estimation performance, [22] proposes an estimator redesign paradigm.

Normally, the working conditions for aggressive maneuvers are more complicated, challenging the applicability of traditional control strategies and uncertainty estimation methods. Therefore, we propose a highly dynamic tracking control strategy with uncertainty smoothing estimation for accurately tracking aggressive trajectories. The main contributions of this paper are summarized as follows:

1) To quicken the response and relieve the actuator burden during high-velocity, large-acceleration flight, a highly dynamic tracking control framework for aggressive maneuvers is proposed.

This work was supported in part by the China Postdoctoral Science Foundation under Grant 2023M731913, in part by the Graduate Research and Innovation Foundation of Chongqing, China under Grant CYB23053, CYB22066, and part by the National Natural Science Foundation of China under Grant 62106027, 52202512. (Corresponding author: Tao Jiang.)

[1]H. Zhang, T. Jiang, and Z. Zheng are with the School of Automation, Chongqing University, Chongqing 400044, China. Email addresses: {zhang_hao, jiangtao_1992, zhizheng}@cqu.edu.cn

[2]J. Ye is with the Department of Computer Science and Technology, Tsinghua University, Beijing, 100084, China. Email address: yejianchuan@yeah.net.

[3]S. Tan is with Collective Intelligence and Collaboration Laboratory, China North Artificial Intelligence and Innovation Research Institute, Beijing, 100084, China. Email address: tristantsq@gmail.com.

2) To mitigate the influence of observer estimation anomalies on control behavior, unlike combinatorial methods [20], [21], an ANESO with adaptive noise suppression and peak attenuation is developed to smoothly estimate the uncertainty.
3) Simulation and real-world experimental comparisons of aggressive trajectory (speed up to 15 m/s and acceleration of 2 g) tracking demonstrate the superiority of the proposed method in terms of tracking accuracy and estimation smoothing.

Notation: In what follows, we define $\mathbb{R}_+ = (0, \infty)$. Given $x \in \mathbb{R}$, $\sigma \in \mathbb{R}_+$, define $\text{sat}_\sigma(x) = \max\{-\sigma, \min\{\sigma, x\}\}$. Given $\boldsymbol{x} \in \mathbb{R}^m$, $\boldsymbol{\sigma} = (\sigma_1, \cdots, \sigma_m) \in \mathbb{R}_+^m$, define $\text{sat}_{\boldsymbol{\sigma}}(\boldsymbol{x}) = (\text{sat}_{\sigma_1}(x_1), \cdots, \text{sat}_{\sigma_m}(x_m))$ and $\text{dz}_{\boldsymbol{\sigma}}(\boldsymbol{x}) = \boldsymbol{x} - \text{sat}_{\boldsymbol{\sigma}}(\boldsymbol{x})$. $\text{diag}(a, \cdots, b)$ is a diagonal matrix. $\text{sgn}(\cdot)$ is the sign function. $\|\cdot\|$ is the Euclidean norm.

II. System Modeling

In this paper, two coordinate systems, inertial frame $\mathcal{F}_\mathcal{I} = [\boldsymbol{x}_I, \boldsymbol{y}_I, \boldsymbol{z}_I]$ and body frame $\mathcal{F}_\mathcal{B} = [\boldsymbol{x}_B, \boldsymbol{y}_B, \boldsymbol{z}_B]$, are first defined. Consider the quadrotor fuselage as a rigid body of mass m and assume that its geometric center coincides with the center of gravity. For the orientation of $\mathcal{F}_\mathcal{B}$ relative to $\mathcal{F}_\mathcal{I}$, the rotation matrix $\boldsymbol{R}(\boldsymbol{q}) \in SO(3)$ parameterized by the quaternion $\boldsymbol{q} = [q_w, q_x, q_y, q_z]^\text{T} \in \mathbb{S}^3$ is given [23]. The position, velocity and acceleration of the quadrotor in $\mathcal{F}_\mathcal{I}$ are indicated by $\boldsymbol{\eta} = [x, y, z]^\text{T}$, $\boldsymbol{v} = [v_x, v_y, v_z]^\text{T}$ and $\boldsymbol{a} = [a_x, a_y, a_z]^\text{T}$, respectively, and the angular velocity in $\mathcal{F}_\mathcal{B}$ is denoted by $\boldsymbol{\omega} = [p, q, r]^\text{T}$.

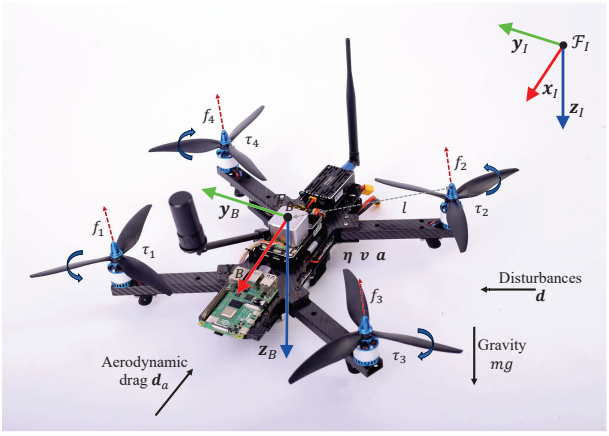

Fig. 2. Variables representation and force analysis.

For quadrotors, the motion can be controlled by the total thrust f and the resultant torque $\boldsymbol{\tau} = [\tau_\phi, \tau_\theta, \tau_\psi]^\text{T}$ generated by the propellers. Applying the Newton-Euler method, the dynamics of a quadrotor is obtained as follows:

$$m\dot{\boldsymbol{v}} = -\boldsymbol{F} + mg\boldsymbol{e}_3 + \boldsymbol{d}_f, \tag{1}$$

$$\dot{\boldsymbol{q}} = \frac{1}{2}\boldsymbol{q} \otimes \begin{bmatrix} 0 \\ \boldsymbol{\omega} \end{bmatrix}, \tag{2}$$

$$\dot{\boldsymbol{\omega}} = \boldsymbol{J}^{-1}\boldsymbol{\tau} + \boldsymbol{d}_l, \tag{3}$$

in which $\boldsymbol{F} = f\boldsymbol{R}(\boldsymbol{q})\boldsymbol{e}_3$ is the equivalent control force; g is the gravity acceleration; $\boldsymbol{e}_3 = [0, 0, 1]^\text{T}$ is a unit vector; $\boldsymbol{d}_f$ denotes the lumped uncertainty of the translational loop (with wind gust, aerodynamic drag $\boldsymbol{d}_a$, etc.); $\otimes$ indicates the quaternion multiplication operator.

$$\boldsymbol{d}_l = \begin{bmatrix} qr(J_{yy} - J_{zz})/J_{xx} + d_{\tau_\phi} \\ pr(J_{zz} - J_{xx})/J_{yy} + d_{\tau_\theta} \\ pq(J_{xx} - J_{yy})/J_{zz} + d_{\tau_\psi} \end{bmatrix} \tag{4}$$

is the lumped uncertainty of the rotational loop, in which $\boldsymbol{d}_\tau = [d_{\tau_\phi}, d_{\tau_\theta}, d_{\tau_\psi}]^\text{T}$ is the unmodeled dynamics (includes external disturbances and aerodynamic torque, etc.); $\boldsymbol{J} = \text{diag}[J_{xx}, J_{yy}, J_{zz}]$ is the inertia matrix.

Quadrotors are subjected to significant aerodynamic drag during aggressive maneuvers, which are modeled as

$$\boldsymbol{d}_a = \begin{bmatrix} -k_x v_{x_B} \\ -k_y v_{y_B} \\ -k_z v_{z_B} + k_h(v_{x_B}^2 + v_{y_B}^2) \end{bmatrix}, \tag{5}$$

where $[v_{x_B}, v_{y_B}, v_{z_B}] = \boldsymbol{R}^\text{T}\boldsymbol{v}$ is the projection of velocity on $\mathcal{F}_\mathcal{B}$; k_i, $i = x, y, z$ and k_h are positive parameters.

The f and $\boldsymbol{\tau}$ are functions of rotor speeds, given as

$$\begin{bmatrix} f \\ \boldsymbol{\tau} \end{bmatrix} = \boldsymbol{G}_1 c_t \boldsymbol{r}^{\circ 2} + \boldsymbol{G}_2 \dot{\boldsymbol{r}}, \tag{6}$$

where c_t denotes the propeller composite thrust coefficient; $\circ$ stands for the Hadamard power; $\boldsymbol{r}$ is the angular speed vector of the propeller. Based on the physical mapping relationship, $\boldsymbol{G}_1$ and $\boldsymbol{G}_2$ are defined as

$$\boldsymbol{G}_1 = \begin{bmatrix} 1 & 1 & 1 & 1 \\ -l\sqrt{2}/2 & l\sqrt{2}/2 & l\sqrt{2}/2 & -l\sqrt{2}/2 \\ l\sqrt{2}/2 & -l\sqrt{2}/2 & l\sqrt{2}/2 & -l\sqrt{2}/2 \\ c_r & c_r & -c_r & -c_r \end{bmatrix}, \tag{7}$$

$$\boldsymbol{G}_2 = \begin{bmatrix} 0 & 0 & 0 & 0 \\ 0 & 0 & 0 & 0 \\ 0 & 0 & 0 & 0 \\ J_r & J_r & -J_r & -J_r \end{bmatrix}, \tag{8}$$

in which c_r denotes the ratio of propeller torque coefficient c_m to c_t; l is the fuselage radius; J_r is the rotational inertia of the rotor and propeller around $\boldsymbol{z}_B$.

Unlike slow flight, aggressive maneuvers are more subject to the conjoint effects of external disturbances, actuator constraints, and complex aerodynamics. Therefore, the control strategy and uncertainty estimation methods need to be improved to achieve accurate tracking of aggressive trajectories in highly dynamic and noisy scenarios.

Assumption 1: Like [17], we assume that the variations of $\boldsymbol{d}_f$ and $\boldsymbol{d}_l$ are bounded and there exist two positive constants $\overline{d}_f$ and $\overline{d}_l$ such that $\|\boldsymbol{d}_f\| \leq \overline{d}_f$ and $\|\boldsymbol{d}_l\| \leq \overline{d}_l$.

III. Main Results

A. Control Architecture

The highly dynamic tracking control method with uncertainty smoothing estimation, which enables accurate tracking of aggressive trajectories, is shown in Fig. 3.

To mitigate the influence of conjoint effects on tracking performance, the ANESO with noise suppression and peak

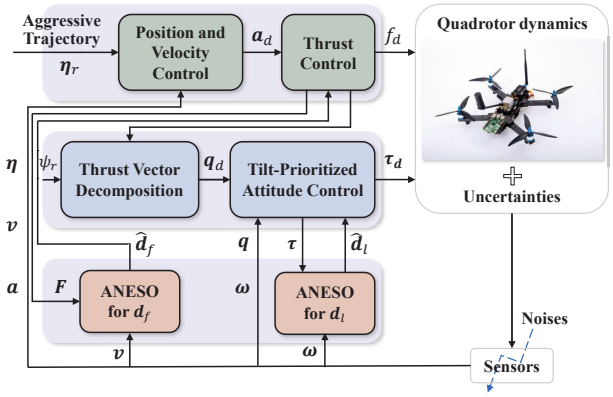

Fig. 3. Block diagram of highly dynamic tracking control.

attenuation is developed to smoothly estimate $\boldsymbol{d}_f$ and $\boldsymbol{d}_l$ during aggressive maneuvers. Combining the estimation results with the translational and rotational subsystems, respectively, effectively compensates for the uncertainty and enhances the control robustness of the system. In addition, to quicken the tracking response and alleviate the actuator burden, higher-order feed-forward information, and tilt-priority control are employed to improve the tracking performance and evade the effect of actuator saturation.

B. Design of ANESO

Inspired by [22], to mitigate the influence of outliers and noise on the estimation behavior of high-gain observers, an ANESO is developed to improve the estimation smoothness of ESO in noisy scenarios.

For the following uncertain second-order system whose model dynamics are partially known:

$$\begin{aligned} \dot{x}_1(t) &= f(\cdot,t)+bu(t)+x_2(t), \\ \dot{x}_2(t) &= h(t), \\ y_1(t) &= x_1(t)+n(t), \end{aligned} \tag{9}$$

in which $x_1(t)$, $u(t)$, b, and $y_1(t)$ are the state, input, input gain, and measured output of the system, respectively; $x_2(t)$ is the extended state that denotes the lumped uncertainty [18] and has derivative $h(t)$; $n(t)$ is the measurement noise; $f(\cdot,t)$ denotes the known model dynamics. To simplify notation, the time variable will be omitted if no confusion is caused.

To achieve smooth estimation of uncertainty, the ANESO is designed as follows:

$$\begin{aligned} \dot{z}_1 &= f(\cdot,t)+bu+z_2+k_1\mathrm{sat}_s\left(\mathrm{dz}_d\left(y_1-z_1\right)\right), \\ \dot{z}_2 &= k_2\mathrm{sat}_s\left(\mathrm{dz}_d\left(y_1-z_1\right)\right), \\ \dot{s} &= -\Lambda_S s+\Theta_S|y_1-z_1|, \\ \dot{d} &= -\Lambda_D d+\Theta_D|y_1-z_1|, \end{aligned} \tag{10}$$

in which k_1 and k_2 denote the observer gains; z_1 and z_2 are the estimation of x_1 and x_2, respectively; s and d are the auxiliary dynamic variables for adaptive saturation and dead-zone, respectively; Λ_S, Θ_S, Λ_D and Θ_D represent adaptation design gains.

The estimation error dynamics can be obtained as

$$\begin{aligned} \dot{\tilde{x}}_1 &= \tilde{x}_2-k_1\tilde{x}_1-k_1\delta, \\ \dot{\tilde{x}}_2 &= h-k_2\tilde{x}_1-k_2\delta, \\ \dot{s} &= -\Lambda_S s+\Theta_S|\tilde{x}_1+n|, \\ \dot{d} &= -\Lambda_D d+\Theta_D|\tilde{x}_1+n|, \end{aligned} \tag{11}$$

in which $\delta=\mathrm{sat}_s\left(\mathrm{dz}_d(\tilde{x}_1+n)\right)-\tilde{x}_1$, $\tilde{x}_1=x_1-z_1$ as well as $\tilde{x}_2=x_2-z_2$.

Theorem 1: For the system (9) and the proposed ANESO (10). Suppose that Assumption 1 is satisfied, and that the initial conditions of ANESO belong to a compact subset of $\mathbb{R}^2$. Then there exist positive k_1, k_2, Λ_S, Θ_S, Λ_D and Θ_D such that ANESO is input-to-state stable.

Proof: The Lyapunov function is defined as

$$\begin{aligned} V_o &= \sqrt{e_o^T P e_o}+\zeta s+\xi d \\ &+ (\zeta+\xi+\eta)\max\left\{\max\left\{|\tilde{x}_1|-d,0\right\}-s,0\right\}, \end{aligned} \tag{12}$$

where $e_o=[\tilde{x}_1,\tilde{x}_2]^{\mathrm{T}}\in\mathbb{R}^2$ denotes the estimation error; ζ, ξ, $\eta\in\mathbb{R}_+$ are positive constants; $P\in\mathbb{R}^{2\times2}$ is the positive definite matrix satisfying $A^{\mathrm{T}}P+PA=-I$ in which $A=[-k_1,1;-k_2,0]\in\mathbb{R}^{2\times2}$ is Hurwitz.

Since $\underline{\lambda}_P I\le P\le\overline{\lambda}_P I$, where $\underline{\lambda}_P\in\mathbb{R}_+$ and $\overline{\lambda}_P\in\mathbb{R}_+$ are the smallest and the largest eigenvalues of P, V_o in (12) is lower bounded as

$$V_o\ \ge\ V_e\ \ge\ \sqrt{\underline{\lambda}_P}\|e_o\|, \tag{13}$$

where $V_e=\sqrt{e_o^{\mathrm{T}}Pe_o}$.

Meanwhile, one has

$$|\tilde{x}_1|\ \le\ l_0V_e\ \le\ l_0\sqrt{\overline{\lambda}_P}\|e_o\|, \tag{14}$$

in which $l_0=1/\sqrt{\underline{\lambda}_P}\in\mathbb{R}_+$, and the upper bound of V_o is obtained as

$$\begin{aligned} V_o &\le \sqrt{\overline{\lambda}_P}\|e_o\|+(\zeta+\xi+\eta)\left(s+d+|\tilde{x}_1|\right) \\ &\le \left(\sqrt{\overline{\lambda}_P}+(\zeta+\xi+\eta)\,l_0\sqrt{\overline{\lambda}_P}\right)\|e_o\| \\ &\quad +(\zeta+\xi+\eta)\left(s+d\right). \end{aligned} \tag{15}$$

The Dini derivative of $|\tilde{x}_1|$ becomes

$$\begin{aligned} D^+|\tilde{x}_1| &\le l_1V_e+\bar{k}|\delta|+\overline{h} \\ &\le \left(\bar{k}l_0+l_1\right)V_e+\bar{k}\overline{n}+\overline{h}, \end{aligned} \tag{16}$$

where $l_1=\|A\|/\sqrt{\underline{\lambda}_P}\in\mathbb{R}_+$, $\bar{k}=\max(k_1,k_2)\in\mathbb{R}_+$, $|h|\le\overline{h}\in\mathbb{R}_+$ and $|n|\le\overline{n}\in\mathbb{R}_+$.

Similarly, the Dini derivative of V_o has

$$D^+V_o\ \le\ -c_1V_e+c_2\left(\bar{k}|\delta|+\overline{h}\right)+g_1\left(\tilde{x}_1,s,d\right), \tag{17}$$

with

$$g_1\left(\tilde{x}_1,s,d\right)=\begin{cases}\zeta s_u+\xi d_u, & |\tilde{x}_1|-d<s\\ -\left(\xi+\eta\right)s_u-\left(\zeta+\eta\right)d_u+\Delta, & |\tilde{x}_1|-d\ge s\end{cases}$$

in which $c_1=1/\overline{\lambda}_P\in\mathbb{R}_+$, $c_2=\overline{\lambda}_P/\sqrt{\underline{\lambda}_P}\in\mathbb{R}_+$, $s_u=-\Lambda_S s+\Theta_S|\tilde{x}_1+n|$, $d_u=-\Lambda_D d+\Theta_D|\tilde{x}_1+n|$ as well as $\Delta=(\zeta+\xi+\eta)\,D^+|\tilde{x}_1|$.

Select $\Theta_S^\star \in \mathbb{R}_+$, $\Theta_D^\star \in \mathbb{R}_+$ and $\eta \in \mathbb{R}_+$ as

$$\begin{aligned}\Theta_S^\star &= \Lambda_S + \frac{c_2\bar{k}}{2(\eta+\xi)},\\ \Theta_D^\star &= \Lambda_D + \frac{c_2\bar{k}}{2(\eta+\zeta)},\\ \eta &= \frac{c_1}{3(\bar{k}l_0+l_1)}.\end{aligned} \tag{18}$$

Then, fix $\Theta_S > \Theta_S^\star$, $\Theta_D > \Theta_D^\star$, and let ζ, ξ be chosen such that

$$\begin{aligned}\zeta\left(\Theta_S l_0 + \bar{k}l_0 + l_1\right) &\le \frac{c_1}{3},\\ \xi\left(\Theta_D l_0 + \bar{k}l_0 + l_1\right) &\le \frac{c_1}{3}.\end{aligned} \tag{19}$$

Subsequently, for some $\nu \in \mathbb{R}_+$, one has

$$c_2\bar{k}|\tilde{x}_1| - (\xi+\eta)s_u - (\zeta+\eta)d_u \le -\nu(s+d). \tag{20}$$

Consequently, there are a_{11}, a_{12}, a_{13}, a_{14}, a_{15}, a_{21}, a_{22}, a_{23}, a_{24} and $a_{25} \in \mathbb{R}_+$ such that

$$D^+V_o \le g_2(V_e, s, d) + g_3\left(\overline{h}, \overline{n}\right), \tag{21}$$

with

$$g_2(V_e,s,d) = \begin{cases} -a_{11}V_e - a_{12}s - a_{13}d, & |\tilde{x}_1| - d < s\\ -a_{21}V_e - a_{22}s - a_{23}d, & |\tilde{x}_1| - d \ge s\end{cases}$$

and

$$g_3\left(\overline{h},\overline{n}\right) = \begin{cases} a_{14}\overline{h} + a_{15}\overline{n}, & |\tilde{x}_1| - d < s\\ a_{24}\overline{h} + a_{25}\overline{n}, & |\tilde{x}_1| - d \ge s\end{cases}$$

where

$$\begin{aligned} a_{11} &= c_1 - (\zeta\Theta_S + \xi\Theta_D)l_0,\\ a_{12} &= \zeta\Lambda_S, a_{13} = \xi\Lambda_D, a_{14} = c_2,\\ a_{21} &= c_1 - (\zeta+\xi+\eta)(\bar{k}l_0 + l_1),\\ a_{22} &= \nu, a_{23} = \nu, a_{24} = c_2 + \zeta + \xi + \eta,\\ a_{15} &= c_2\bar{k} + \zeta\Theta_S + \xi\Theta_D,\\ a_{25} &= (c_2 + \zeta + \xi + \eta)\bar{k}.\end{aligned}$$

Thus, for some $a_1, a_2, a_3 \in \mathbb{R}_+$, D^+V_o can meet

$$D^+V_o \le -a_1V_o + a_2\overline{h} + a_3\overline{n}. \tag{22}$$

From (13), (15), (16), (22), as well as the definitions and lemmas about ISS in [24], the proposed ANESO is input-to-state stable, and the estimation error $\tilde{x}_2$ is bounded. ■

Remark 1: The advantages of ANESO over conventional ESOs are: i) ESOs amplify measurement noise, leading to undesirable actions of controllers and abrasions of actuators; and ii) excessive peaks in ESO estimation directly lead to actuator saturation failure. Compared to the above, ANESO provides a smoothing guarantee for uncertainty estimation by introducing adaptive nonlinear terms for noise suppression and peak attenuation. Moreover, unlike fixed saturation and dead-zone levels, these values can be adaptively adjusted to achieve the desired effect.

C. Translational Subsystem

1) Disturbance Estimation: Unlike slow flight, conditions for aggressive maneuvering are more complicated and place higher demands on compensation for uncertainty. To ensure that the uncertainty is smoothly compensated, the ANESO designed in the translation loop enables smooth estimation of the uncertainty $\boldsymbol{d}_f$.

Let $\boldsymbol{x}_3 = \boldsymbol{v}$, $\boldsymbol{d}_f$ as the extended state $\boldsymbol{x}_4$ and $\dot{\boldsymbol{d}}_f = \boldsymbol{h}_f$. Then the position dynamics (1) can be rewritten as

$$\begin{aligned}\dot{\boldsymbol{x}}_3 &= \frac{-\boldsymbol{F}}{m} + g\boldsymbol{e}_3 + \frac{\boldsymbol{x}_4}{m},\\ \dot{\boldsymbol{x}}_4 &= \boldsymbol{h}_f.\end{aligned} \tag{23}$$

Like (10), the following ANESO is employed to estimate $\boldsymbol{d}_f$, thus

$$\begin{aligned}\dot{\boldsymbol{z}}_3 &= \frac{-\boldsymbol{F}}{m} + g\boldsymbol{e}_3 + \frac{\boldsymbol{z}_4}{m} + \boldsymbol{k}_3\mathrm{sat}_{\boldsymbol{s}_p}\left(\mathrm{dz}_{\boldsymbol{d}_p}(\boldsymbol{y}_3 - \boldsymbol{z}_3)\right),\\ \dot{\boldsymbol{z}}_4 &= \boldsymbol{k}_4\mathrm{sat}_{\boldsymbol{s}_p}\left(\mathrm{dz}_{\boldsymbol{d}_p}(\boldsymbol{y}_3 - \boldsymbol{z}_3)\right),\\ \dot{\boldsymbol{s}}_p &= -\boldsymbol{\Lambda}_{S_p}\boldsymbol{s}_p + \boldsymbol{\Theta}_{S_p}|\boldsymbol{y}_3 - \boldsymbol{z}_3|,\\ \dot{\boldsymbol{d}}_p &= -\boldsymbol{\Lambda}_{D_p}\boldsymbol{d}_p + \boldsymbol{\Theta}_{D_p}|\boldsymbol{y}_3 - \boldsymbol{z}_3|,\end{aligned} \tag{24}$$

in which $\boldsymbol{z}_3$, $\boldsymbol{z}_4$ denote the estimation of $\boldsymbol{x}_3$, $\boldsymbol{x}_4$, respectively; $\boldsymbol{k}_3$, $\boldsymbol{k}_4 \in \mathbb{R}^{3\times3}$ are the observer diagonal gain matrices; $\boldsymbol{y}_3$ denotes the measured output of $\boldsymbol{x}_3$ with noise $\boldsymbol{n}_3$; $\boldsymbol{s}_p$, $\boldsymbol{d}_p$ are the auxiliary dynamic variables for adaptive saturation and dead-zone, respectively; $\boldsymbol{\Lambda}_{S_p}$, $\boldsymbol{\Theta}_{S_p}$, $\boldsymbol{\Lambda}_{D_p}$ and $\boldsymbol{\Theta}_{D_p}$ represent adaption design gains.

2) Position and Velocity Control: To expedite the response and achieve rapid tracking of highly dynamic trajectories, the tracking controller is mathematically equivalent as follows:

$$\boldsymbol{a}_d = \boldsymbol{k}_\eta\boldsymbol{e}_\eta + \boldsymbol{k}_v\boldsymbol{e}_v + \boldsymbol{k}_a\boldsymbol{e}_a + \ddot{\boldsymbol{\eta}}_r, \tag{25}$$

in which $\boldsymbol{e}_\eta = \boldsymbol{\eta}_r - \boldsymbol{\eta}$, $\boldsymbol{e}_v = \dot{\boldsymbol{\eta}}_r - \boldsymbol{v}$, $\boldsymbol{e}_a = \ddot{\boldsymbol{\eta}}_r - \boldsymbol{a}$ are feedback terms; $\boldsymbol{\eta}_r$ is the desired trajectory; $\boldsymbol{k}_\eta$, $\boldsymbol{k}_v$ and $\boldsymbol{k}_a \in \mathbf{R}^{3\times3}$ denote the positive-definite diagonal gain matrices; $\boldsymbol{a}_d$ is the desired acceleration.

Remark 2: Higher order information derived directly from the desired trajectory enhances the tracking response. Moreover, $\boldsymbol{k}_a\boldsymbol{e}_a$ can be interpreted as the differential term in PID control, which is beneficial to mitigate the sensitivity of the system to abrupt injections or fast-varying disturbances, thus improving the performance of the control system.

3) Thrust Control: With the above $\boldsymbol{a}_d$ and $\hat{\boldsymbol{d}}_f$, from (1), (24) and (25), the f_d and $\boldsymbol{z}_{B_d}$ are obtained as

$$f_d\boldsymbol{z}_{B_d} = m(-\boldsymbol{a}_d + g\boldsymbol{e}_3) + \hat{\boldsymbol{d}}_f. \tag{26}$$

Given reference heading angle ψ_r, we define an intermediate axis $\boldsymbol{y}_{C_d} = [-\sin\psi_r, \cos\psi_r, 0]$, by which the desired attitude are as follows:

$$\boldsymbol{x}_{B_d} = \frac{-\boldsymbol{z}_{B_d}\times\boldsymbol{y}_{C_d}}{\|\boldsymbol{z}_{B_d}\times\boldsymbol{y}_{C_d}\|}, \tag{27}$$

$$\boldsymbol{y}_{B_d} = -\boldsymbol{x}_{B_d}\times\boldsymbol{z}_{B_d}, \tag{28}$$

$$\boldsymbol{R}(\boldsymbol{q}_d) = \left[\boldsymbol{x}_{B_d}, \boldsymbol{y}_{B_d}, \boldsymbol{z}_{B_d}\right], \tag{29}$$

in which $\boldsymbol{R}(\boldsymbol{q}_d) \in \mathbf{R}^{3\times3}$ is the desired attitude expressed by the desired quaternion $\boldsymbol{q}_d$.

D. Rotational Subsystem

1) Disturbance Estimation: As in (9), let $\boldsymbol{x}_5 = \boldsymbol{\omega}$, $\boldsymbol{d}_l$ as the extended state $\boldsymbol{x}_6$ and $\dot{\boldsymbol{d}}_l = \boldsymbol{h}_l$, and then the attitude dynamics in (3) can be rewritten as:

$$\begin{aligned} \dot{\boldsymbol{x}}_5 &= \boldsymbol{J}^{-1}\boldsymbol{\tau} + \boldsymbol{x}_6, \\ \dot{\boldsymbol{x}}_6 &= \boldsymbol{h}_l. \end{aligned} \tag{30}$$

Like (10), the following ANESO is developed to estimate the uncertainty $\boldsymbol{d}_l$, thus

$$\begin{aligned} \dot{\boldsymbol{z}}_5 &= \boldsymbol{J}^{-1}\boldsymbol{\tau} + \boldsymbol{z}_6 + \boldsymbol{k}_5 \mathrm{sat}_{\boldsymbol{s}_a}\left(\mathrm{dz}_{\boldsymbol{d}_a}\left(\boldsymbol{y}_5 - \boldsymbol{z}_5\right)\right), \\ \dot{\boldsymbol{z}}_6 &= \boldsymbol{k}_6 \mathrm{sat}_{\boldsymbol{s}_a}\left(\mathrm{dz}_{\boldsymbol{d}_a}\left(\boldsymbol{y}_5 - \boldsymbol{z}_5\right)\right), \\ \dot{\boldsymbol{s}}_a &= -\boldsymbol{\Lambda}_{S_a}\boldsymbol{s}_a + \boldsymbol{\Theta}_{S_a}|\boldsymbol{y}_5 - \boldsymbol{z}_5|, \\ \dot{\boldsymbol{d}}_a &= -\boldsymbol{\Lambda}_{D_a}\boldsymbol{d}_a + \boldsymbol{\Theta}_{D_a}|\boldsymbol{y}_5 - \boldsymbol{z}_5|, \end{aligned} \tag{31}$$

in which $\boldsymbol{z}_5$, $\boldsymbol{z}_6$ denote the estimation of $\boldsymbol{x}_5$, $\boldsymbol{x}_6$, respectively; $\boldsymbol{k}_5$, $\boldsymbol{k}_6 \in \mathbb{R}^{3\times 3}$ are the observer diagonal gain matrices; $\boldsymbol{y}_5$ denotes the measured output of $\boldsymbol{x}_5$ with noise $\boldsymbol{n}_5$; $\boldsymbol{s}_a$, $\boldsymbol{d}_a$ are the auxiliary dynamic variables for adaptive saturation and dead-zone, respectively; $\boldsymbol{\Lambda}_{S_a}$, $\boldsymbol{\Theta}_{S_a}$, $\boldsymbol{\Lambda}_{D_a}$ and $\boldsymbol{\Theta}_{D_a}$ represent adaption design gains.

2) Tilt-Prioritized Attitude Control: Owing to the physical limitations of the rotor, it is difficult to generate both the required thrust and reaction torque when performing aggressive maneuvers or recovering from large errors. Therefore, tilt-priority attitude control inspired by [25] is utilized to regulate the reduced attitude (pitch and roll) error $\tilde{\boldsymbol{q}}_{e_t}$ and yaw error $\tilde{\boldsymbol{q}}_{e_y}$, respectively, while avoiding saturation, as follows:

$$\boldsymbol{q}_e = \boldsymbol{q}_d \otimes \boldsymbol{q}^{-1}, \tag{32}$$

$$\tilde{\boldsymbol{q}}_{e_t} = \frac{1}{\sqrt{q_{e_w}^2 + q_{e_z}^2}} \begin{bmatrix} q_{e_w}q_{e_x} - q_{e_y}q_{e_z} \\ q_{e_w}q_{e_y} + q_{e_x}q_{e_z} \\ 0 \end{bmatrix}, \tag{33}$$

$$\tilde{\boldsymbol{q}}_{e_y} = \frac{1}{\sqrt{q_{e_w}^2 + q_{e_z}^2}} \begin{bmatrix} 0 & 0 & q_{e_w} \end{bmatrix}^{\mathrm{T}}, \tag{34}$$

where $\boldsymbol{q}_e = \left[q_{e_w}, q_{e_x}, q_{e_y}, q_{e_z}\right]^{\mathrm{T}}$ is the attitude error.

The desired angular acceleration $\boldsymbol{\alpha}_d$ can be calculated by the following control law:

$$\boldsymbol{\alpha}_d = \boldsymbol{k}_{q_t}\tilde{\boldsymbol{q}}_{e_t} + \boldsymbol{k}_{q_y}\mathrm{sgn}\left(q_{e_w}\right)\tilde{\boldsymbol{q}}_{e_y} + \boldsymbol{k}_{\omega}\left(\boldsymbol{\omega}_r - \boldsymbol{\omega}\right), \tag{35}$$

where $\boldsymbol{k}_{q_t}$ and $\boldsymbol{k}_{q_y}$ are positive gains for reduced-attitude and yaw control, respectively; $\boldsymbol{k}_{\omega}$ is the positive-definite diagonal gain matrix; $\boldsymbol{\omega}_r$ denotes the desired angular velocity.

Therefore, the desired torque as

$$\boldsymbol{\tau}_d = \boldsymbol{J}\left(\boldsymbol{\alpha}_d - \hat{\boldsymbol{d}}_l\right). \tag{36}$$

Remark 3: Heading control is less efficient than pitch and roll due to the different working mechanisms and tends to lead to motor saturation. Fortunately, the thrust direction that dominates quadrotor trajectory tracking is independent of its heading angle. Therefore, the tilt-priority control strategy ensures accurate position tracking when the system capacity is limited or degraded.

IV. Application Simulation and Experimental Examples

In what follows, the superiority of the proposed method to track aggressive trajectories (with velocity up to 15 m/s and acceleration of 2 g) is verified through extensive comparative simulations and real-world experiments.

A. Numerical Simulation

During actual flight, external disturbances and internal noise inevitably affect the tracking performance. Therefore, these two cases are directly incorporated into the numerical simulation environment to fully validate the capability of the proposed solution in tracking aggressive trajectories.

1) Noise Suppression and Peak Attenuation: Comparative results of ANESO and ESO estimates are plotted in Figs. 4 and 5. The behavior of the steady-state is essentially identical for both observers. However, the ESO exhibits severe high-frequency oscillations and peaks. Superior to ESO, ANESO can effectively suppress noise and attenuation peaks, and achieve smooth estimation of uncertainty.

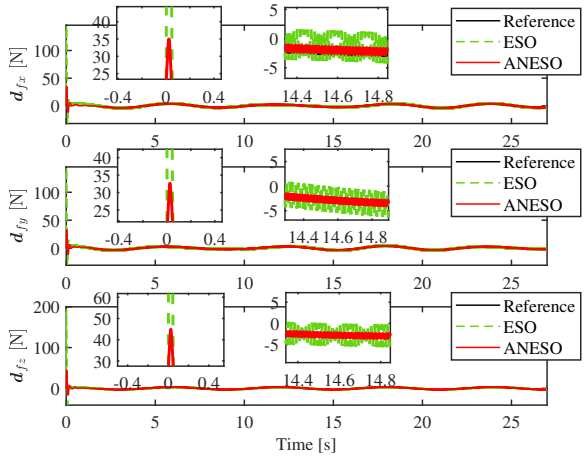

Fig. 4. Comparison of estimation results for $\boldsymbol{d}_f$.

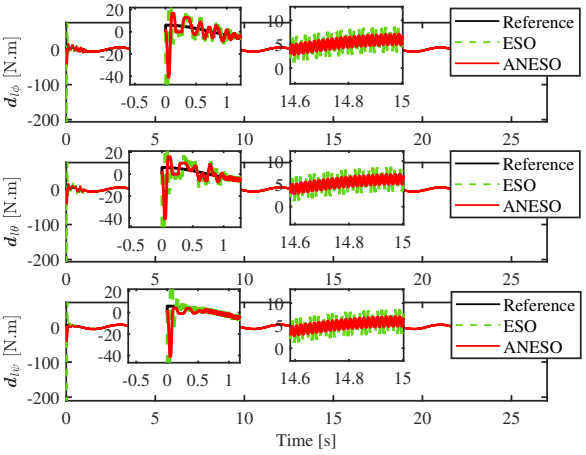

Fig. 5. Comparison of estimation results for $\boldsymbol{d}_l$.

TABLE I: Tracking Performance Comparison

	MD [m]		RMSE [m]		Response time [s]	
	x	y	x	y	x	y
PID	0.757	0.736	0.545	0.507	2.319	1.553
TC + ESO	0.688	0.705	0.395	0.419	0.941	0.963
Proposed	0.498	0.164	0.247	0.106	0.525	0.592

2) Tracking Performance: Figs. 6 and 7 provide the simulation results of tracking aggressive trajectories employing PID, TC + ESO (combination of the proposed controller and conventional ESO), and the proposed method. The maximum deviation (MD) and root-mean-square-error (RMSE) of the position as the metrics of tracking accuracy. Comparison of different control methods in terms of tracking accuracy and response speed is listed in Table I. Clearly, for aggressive trajectories, the proposed method has the fastest response and higher tracking accuracy. Moreover, in Fig. 6, the maximum velocity and acceleration are 14.2 m/s and 19.8 m/s^2 (2.02 g), respectively, while the tracking effect of the proposed method is smoother.

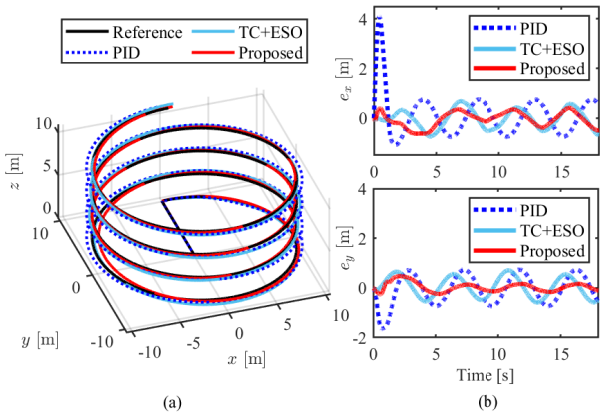

Fig. 6. Tracking results. (a) Trajectory. (b) Tracking error.

B. Real-World Experiment

In the following, the experimental results of outdoor real-world high dynamic flight are presented. Different from ideal indoor scenarios, we evaluate the tracking performance of the proposed scheme in natural wind fields at the velocities shown in Fig. 10.

1) Experimental Setup: The experimental platform shown in Fig. 8 is utilized to verify the effectiveness of the proposed approach. The self-developed X390 flight platform with an avionic system consisting of LiPo batteries, electronic speed controllers, and motors with three-bladed propellers. And the platform is equipped with an autopilot and a Raspberry Pi. Positioning and state information of the quadrotor is provided in real-time by the C-RTK and the inertial measurement unit. Over a WiFi network, the ground station is responsible for remotely accessing the Raspberry Pi and publishing desired commands.

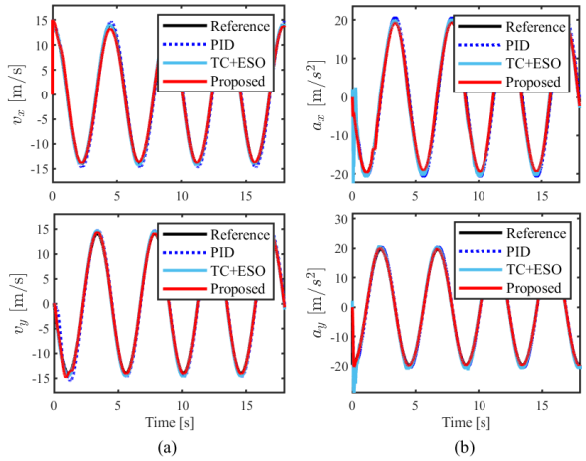

Fig. 7. High-speed maneuvering at speeds up to 15 m/s with 2 g acceleration. (a) Velocity. (b) Acceleration.

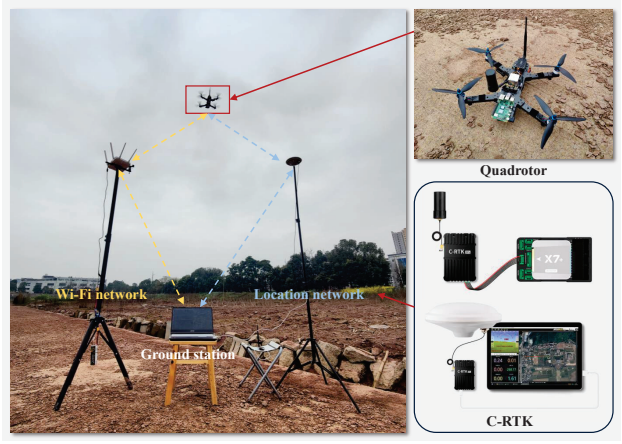

Fig. 8. Outdoor experimental platforms.

2) Actual Flight Results: Unlike indoor scenarios, quadrotors encounter more complex wind conditions during outdoor testing, and the highly dynamic flights also induce stronger aerodynamic drag. Fig. 9 and Fig. 10 represent the trajectory tracking situation and velocity zones for real flights outdoors, respectively. Table II indicates that the tracking accuracy of the proposed scheme is better than the previous two, showing stronger tracking capability.

V. CONCLUSIONS

In this paper, a tracking control method with uncertainty smoothing estimation is proposed to achieve accurate tracking of aggressive trajectories with velocities up to 15 m/s

TABLE II: Comparison of Actual Flight Experiments

	MD [m]		RMSE [m]	
	x	y	x	y
PID	3.007	2.961	1.373	1.359
TC+ESO	2.134	2.216	1.137	1.008
Proposed	1.281	1.301	0.573	0.557

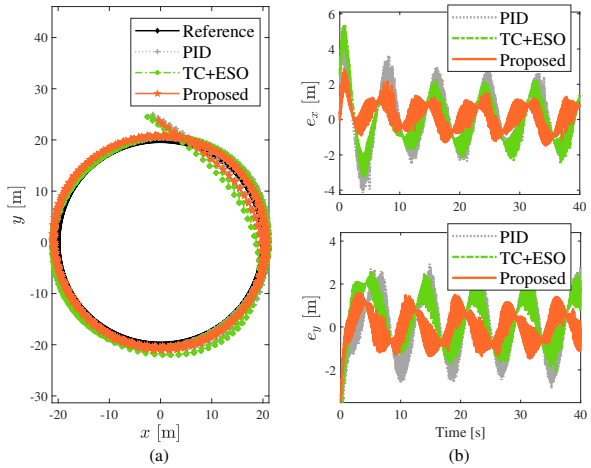

Fig. 9. High-speed follow-the-circle flight. (a) Trajectory. (b) Tracking error.

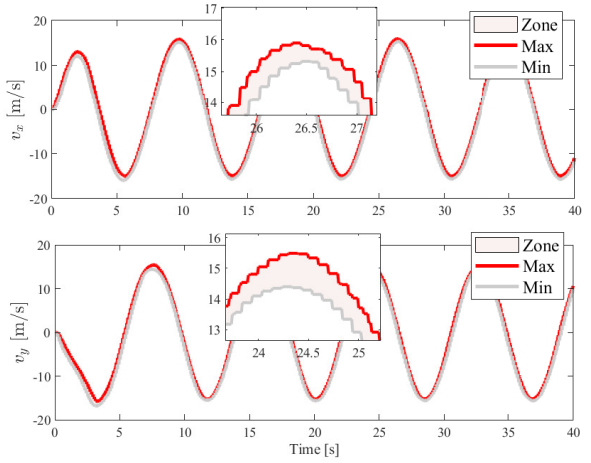

Fig. 10. Velocity zones during aggressive maneuvers.

and accelerations of 2 g. To alleviate the conjoint effect on flight control, a novel ANESO with noise suppression and peak attenuation is proposed for smooth estimation of time-varying uncertainty. Meanwhile, the proposed method accelerates the tracking response and avoids actuator saturation. Finally, extensive simulations and real-world experiments are conducted to evaluate the superiority of the proposed method in terms of tracking accuracy and estimation smoothing.

REFERENCES

[1] Bara J. Emran and H. Najjaran, "A review of quadrotor: An underactuated mechanical system," *Annual Reviews in Control*, vol. 46, pp. 165–180, 2018.

[2] D. Hu, Z. Pei, J. Shi and Z. Tang, "Design, Modeling and Control of a Novel Morphing Quadrotor," *IEEE Robotics and Automation Letters*, vol. 6, no. 4, pp. 8013–8020, 2021.

[3] A. Akhtar, S. Saleem and J. Shan, "Path Following of a Quadrotor With a Cable-Suspended Payload," *IEEE Transactions on Industrial Electronics*, vol. 70, no. 2, pp. 1646–1654, 2023.

[4] H. Liu, D. Liu and Y. Lyu, "Completely Distributed Time-Varying Formation Target Tracking for Quadrotor Team via Image-Based Visual Servoing," *IEEE Transactions on Vehicular Technology*, vol. 71, no. 1, pp. 21–32, 2022.

[5] H. Li, H. Wang, C. Feng, F. Gao, B. Zhou and S. Shen, "AutoTrans: A Complete Planning and Control Framework for Autonomous UAV Payload Transportation," *IEEE Robotics and Automation Letters*, vol. 8, no. 10, pp. 6859–6866, 2023.

[6] Q. Wang, D. Wang, C. Xu, A. Gao and F. Gao, "Polynomial-Based Online Planning for Autonomous Drone Racing in Dynamic Environments," *2023 IEEE/RSJ International Conference on Intelligent Robots and Systems (IROS)*, pp. 1078–1085, 2023.

[7] Y. Zhu, L. Guo, J. Qiao and W. Li, "An enhanced anti-disturbance attitude control law for flexible spacecrafts subject to multiple disturbances," *Control Engineering Practice*, vol. 84, pp. 274–283, 2019.

[8] Q. Sun, J. Fang, W. Zheng and Y. Tang, "Aggressive Quadrotor Flight Using Curiosity-Driven Reinforcement Learning," *IEEE Transactions on Industrial Electronics*, vol. 69, no. 12, pp. 13838–13848, 2022.

[9] E. Tal and S. Karaman, "Accurate Tracking of Aggressive Quadrotor Trajectories Using Incremental Nonlinear Dynamic Inversion and Differential Flatness," *IEEE Transactions on Control Systems Technology*, vol. 29, no. 3, pp. 1203–1218, 2021.

[10] Z. Liu and L. Cai, "Large-angle and High-speed Trajectory Tracking Control of a Quadrotor UAV based on Reachability," *2022 International Conference on Robotics and Automation (ICRA)*, pp. 1983–1988, 2022.

[11] D. Mellinger and V. Kumar, "Minimum snap trajectory generation and control for quadrotors," *2011 IEEE International Conference on Robotics and Automation (ICRA)*, pp. 2520–2525, 2011.

[12] M. Faessler, A. Franchi and D. Scaramuzza, "Differential Flatness of Quadrotor Dynamics Subject to Rotor Drag for Accurate Tracking of High-Speed Trajectories," *IEEE Robotics and Automation Letters*, vol. 3, no. 2, pp. 620–626, 2018.

[13] X. Yu, X. Zhou, K. Guo, J. Jia, L. Guo and Y. Zhang, "Safety Flight Control for a Quadrotor UAV Using Differential Flatness and Dual-Loop Observers," *IEEE Transactions on Industrial Electronics*, vol. 69, no. 12, pp. 13326–13336, 2022.

[14] D. Hanover, P. Foehn, S. Sun, E. Kaufmann and D. Scaramuzza, "Performance, Precision, and Payloads: Adaptive Nonlinear MPC for Quadrotors," *IEEE Robotics and Automation Letters*, vol. 7, no. 2, pp. 690–697, 2022.

[15] D. Wang, Q. Pan, Y. Shi, J. Hu and C. Zhao, "Efficient Nonlinear Model Predictive Control for Quadrotor Trajectory Tracking: Algorithms and Experiment," *IEEE Transactions on Cybernetics*, vol. 51, no. 10, pp. 5057–5068, 2021.

[16] M. Hossny, A. El-Badawy and R. Hassan, "Fuzzy Model Predictive Control of a Quadrotor Unmanned Aerial Vehicle," *2020 International Conference on Unmanned Aircraft Systems (ICUAS)*, pp. 1704–1713, 2020.

[17] H. Hua, Y. Fang, X. Zhang and B. Lu, "A Novel Robust Observer-Based Nonlinear Trajectory Tracking Control Strategy for Quadrotors," *IEEE Transactions on Control Systems Technology*, vol. 29, no. 5, pp. 1952–1963, 2021.

[18] K. Zhao, J. Zhang, D. Ma and Y. Xia, "Composite Disturbance Rejection Attitude Control for Quadrotor With Unknown Disturbance," *IEEE Transactions on Industrial Electronics*, vol. 67, no. 8, pp. 6894–6903, 2020.

[19] J. Han, "From PID to Active Disturbance Rejection Control," *IEEE Transactions on Industrial Electronics*, vol. 56, no. 3, pp. 900–906, 2009.

[20] H. Sun, R. Madonski, S. Li, Y. Zhang and W. Xue, "Composite Control Design for Systems With Uncertainties and Noise Using Combined Extended State Observer and Kalman Filter," *IEEE Transactions on Industrial Electronics*, vol. 69, no. 4, pp. 4119–4128, 2022.

[21] Y. Du, W. Cao and J. She, "Analysis and Design of Active Disturbance Rejection Control With an Improved Extended State Observer for Systems With Measurement Noise," *IEEE Transactions on Industrial Electronics*, vol. 70, no. 1, pp. 855–865, 2023.

[22] D. Astolfi, A. Alessandri and L. Zaccarian, "Stubborn and Dead-Zone Redesign for Nonlinear Observers and Filters," *IEEE Transactions on Automatic Control*, vol. 66, no. 2, pp. 667–682, 2021.

[23] G. Michieletto, A. Cenedese, L. Zaccarian and A. Franchi, "Hierarchical nonlinear control for multi-rotor asymptotic stabilization based on zero-moment direction," *Automatica*, vol. 117, pp. 108991, 2020.

[24] H. K. Khalil, *Nonlinear Systems*, 3rd ed. Upper Saddle River, NJ, USA: Prentice-Hall, 2002.

[25] D. Brescianini and R. D'Andrea, "Tilt-Prioritized Quadrocopter Attitude Control," *IEEE Transactions on Control Systems Technology*, vol. 28, no. 2, pp. 376–387, Mar. 2020.